

BEYOND MODEL RANKING: PREDICTABILITY-ALIGNED EVALUATION FOR TIME SERIES FORECASTING

Wanjin Feng & Yuan Yuan & Jingtao Ding & Yong Li

Tsinghua University

wanjin.feng@outlook.com y-yuan20@tsinghua.org.cn

ABSTRACT

In the era of increasingly complex AI models for time series forecasting, progress is often measured by marginal improvements on benchmark leaderboards. However, this approach suffers from a fundamental flaw: standard evaluation metrics conflate a model’s performance with the data’s intrinsic unpredictability. To address this pressing challenge, we introduce a novel, predictability-aligned diagnostic framework grounded in spectral coherence. Our framework makes two primary contributions: the **Spectral Coherence Predictability (SCP)**, a computationally efficient ($O(N \log N)$) and task-aligned score that quantifies the inherent difficulty of a given forecasting instance, and the **Linear Utilization Ratio (LUR)**, a frequency-resolved diagnostic tool that precisely measures how effectively a model exploits the linearly predictable information within the data. We validate our framework’s effectiveness and leverage it to reveal two core insights. First, we provide the first systematic evidence of “predictability drift”, demonstrating that a task’s forecasting difficulty varies sharply over time. Second, our evaluation reveals a key architectural trade-off: complex models are superior for low-predictability data, whereas linear models are highly effective on more predictable tasks. We advocate for a paradigm shift, moving beyond simplistic aggregate scores toward a more insightful, predictability-aware evaluation that fosters fairer model comparisons and a deeper understanding of model behavior.

1 INTRODUCTION

Despite the proliferation of ever-more-complex models for time-series forecasting, true progress in the field remains notoriously difficult to measure (Bergmeir, 2024). The community relies on standard metrics, such as Mean Squared Error (MSE) and Mean Absolute Error (MAE), which quantify the magnitude of prediction errors but fail to reveal their origin. These metrics obscure a critical distinction: is a model failing because of its own limitations, or has it hit the fundamental ceiling of what is predictable in the data (Ehrenberg & Bound, 1993)? This ambiguity creates a severe evaluation dilemma, where a sophisticated model on a chaotic series may appear worse than a simple one. It also stalls scientific progress by wasting significant computational resources on problems where gains are impossible. Disentangling model inadequacy from intrinsic data unpredictability is therefore one of the most pressing challenges in the field today (Erkintalo, 2015).

The ideal solution to this dilemma is to first quantify a time series’ intrinsic predictability and then evaluate a model’s performance relative to this established baseline. However, designing a predictability metric that is fit for the modern deep learning forecasting paradigm presents a series of formidable challenges (Pennekamp et al., 2019). First, such a metric must be task-aligned, meaning its theoretical foundation should cohere with multi-horizon forecasting under a squared-error loss, rather than traditional single-step classification accuracy (Mishra & Palanisamy, 2018). Second, it must be computationally efficient to handle the massive, high-dimensional time series prevalent today (Fiecas et al., 2019). Finally, a single, global predictability score is insufficient; a truly useful tool must be diagnostic, offering insights to reveal where a model succeeds or fails in capturing predictable patterns.

Viewed through the lens of these challenges, existing tools are ill-suited for this purpose. Traditional proxies for predictability, such as entropy-rate estimators and Lempel-Ziv complexity, suffer from a fundamental paradigm mismatch (Aboy et al., 2006). These information-theoretic methods were developed for symbolic dynamics and classification tasks, designed to estimate an upper bound on next-symbol accuracy under a 0-1 loss, not a lower bound on multi-step regression error (Zhao et al., 2021). Furthermore, they often assume stationarity and are computationally expensive, which typically entails quadratic-to-cubic time complexity, rendering them impractical for the large-scale, non-stationary datasets common in modern applications (Kontoyiannis et al., 2002; Wyner & Ziv, 2002). An entirely new framework is thus urgently needed to bridge the significant gap between classical predictability theory and contemporary forecasting practice.

To bridge this gap, we introduce a novel diagnostic framework grounded in spectral coherence that is computationally efficient, directly aligned with the MSE objective, and provides rich, multi-scale insights. Our framework consists of two core components: 1) **Spectral Coherence Predictability (SCP)**, a per-instance predictability score \mathcal{P} derived from a linear MSE lower bound, MSE_{lb} . It is computed in $O(N \log N)$ time and is intrinsically consistent with the MSE objective. 2) **Linear Utilization Ratio (LUR)**, a frequency-resolved diagnostic that quantifies how effectively a model exploits linearly predictable information across different spectral bands, enabling fine-grained assessments of under-use, saturation, and beyond-linear gains. With this framework, we aim to shift the time-series evaluation paradigm from simple “model ranking” toward a more profound analysis of “model-data diagnostics,” thereby providing clear, actionable guidance for developing more powerful and reliable forecasting models. Through extensive experiments on synthetic and real-world benchmarks, we validate our proposed framework. We demonstrate that our predictability score is well-calibrated and strongly correlates with the empirical performance of state-of-the-art models. Furthermore, our diagnostics uncover the highly time-varying nature of predictability, enabling a fairer, stratified evaluation that uncovers the differential strengths of different architectures, moving beyond the limitations of aggregate scores.

In summary, our contributions are as follows:

- We are the first to systematically address the evaluation ambiguity in modern time-series forecasting by introducing a framework to decouple model error from a time series’ intrinsic, irreducible unpredictability.
- We propose a computationally efficient and task-aligned Spectral Coherence Predictability (SCP). It provides a per-instance predictability score with a corresponding error lower bound and a frequency-resolved diagnostic to analyze a model’s information utilization.
- Extensive experiments validates this framework’s alignment with state-of-the-art models. We then use it to reveal novel insights like “predictability drift” and introduce a stratified evaluation that uncovers the complementary strengths of different models.

2 RELATED WORK

Our work is positioned at the intersection of two key research areas: the quantification of sequence predictability and the use of spectral methods for time-series analysis.

Predictability of Time Series. Entropy-based notions have long been used to proxy sequence predictability, from Shannon’s entropy and entropy rate to variants usable on continuous data (approximate, sample, fuzzy, and permutation entropy) (Shannon, 1948; Pincus, 1991; Richman & Moorman, 2000; Bandt & Pompe, 2002; Garland et al., 2014). Compression-driven estimators (e.g., Lempel-Ziv) provide nonparametric estimates of entropy rate for symbolic, stationary sources (Ziv & Lempel, 1977). These approaches have also been popular in human mobility, where spatio-temporal regularity supports predictability limits under coarse symbolizations (González et al., 2008; Song et al., 2010; Wang et al., 2021). However, they face three key limitations for general forecasting: (i) computational burden the need for discretization of continuous data; (ii) theoretical misalignment with multi-step squared-loss objectives; and (iii) sensitivity of differential entropy to reparameterization and divergence issues in non-stationary settings (Mohammed et al., 2024). Consequently, existing predictability proxies fail to provide a task-aligned and reliable estimate of the achievable error lower bound for multi-step time-series forecasting.

Spectral Analysis in Time Series Forecasting. Spectral analysis is a cornerstone of time-series modeling, inspiring many recent deep learning architectures. For instance, Autoformer was designed with an auto-correlation mechanism to discover period-based dependencies efficiently (Wu et al., 2021). FEDformer directly integrates Fourier/Wavelet transforms into attention for frequency-domain computation with reduced complexity (Zhou et al., 2022). TimesNet captures complex multi-periodicity by transforming the 1D time series into a 2D representation for analysis (Wu et al., 2023). These methods all leverage spectral properties to build better models. In contrast, our work uses spectral coherence to build a novel diagnostic framework for analyzing data predictability and evaluating the utilization of existing models.

3 PRELIMINARIES

Problem setup and notation. We focus on a setting in which an observed sequence is decomposed into a past (history) portion used as input and a future portion serving as ground-truth for evaluation. Formally, a sample consists of a history $\mathbf{x} \in \mathbb{R}^N$ and a future $\mathbf{y} \in \mathbb{R}^N$ drawn from a distribution \mathbb{D} . The goal is to learn a measurable predictor $f: \mathbb{R}^N \rightarrow \mathbb{R}^N$ that produces a forecast $\hat{\mathbf{y}} = f(\mathbf{x})$. We evaluate predictions with the mean squared error (MSE) per forecast step:

$$\text{MSE}(f; \mathbf{x}, \mathbf{y}) = \frac{1}{N} \|\mathbf{f}(\mathbf{x}) - \mathbf{y}\|_2^2, \quad (1)$$

where $\|\cdot\|_2$ denotes the Euclidean norm. The learning objective is to minimize the expected risk $\mathbb{E}_{(\mathbf{x}, \mathbf{y}) \sim \mathcal{D}}[\text{MSE}(f; \mathbf{x}, \mathbf{y})]$.

Intrinsic predictability via Bayes risk. Under the MSE metric, the risk-minimizing predictor is the conditional expectation $f^*(\mathbf{x}) = \mathbb{E}[\mathbf{y} | \mathbf{x}]$ (Chen et al., 2016). The corresponding minimum achievable risk (Bayes risk) is

$$\text{MSE}^* = \mathbb{E} \left[\frac{1}{N} \|\mathbf{y} - \mathbb{E}[\mathbf{y} | \mathbf{x}]\|_2^2 \right]. \quad (2)$$

This quantity captures the irreducible uncertainty in \mathbf{y} given \mathbf{x} . We use the unconditional variance of the target as a baseline:

$$\text{Var}(\mathbf{y}) = \mathbb{E} \left[\frac{1}{N} \|\mathbf{y} - \mathbb{E}[\mathbf{y}]\|_2^2 \right]. \quad (3)$$

The intrinsic predictability is then defined as

$$\mathcal{P}_{xy}^* = 1 - \frac{\text{MSE}^*}{\text{Var}(\mathbf{y})}, \quad (4)$$

which coincides with the theoretical coefficient of determination (R^2). By the law of total variance, $\text{Var}(\mathbf{y}) = \text{MSE}^* + \text{Var}(\mathbb{E}[\mathbf{y} | \mathbf{x}])$, hence $\mathcal{P}^* \in [0, 1]$. At the extremes, $\mathcal{P}^* = 1$ if and only if $\text{Var}(\mathbf{y} | \mathbf{x}) = 0$ almost surely, i.e., \mathbf{y} is a deterministic function of \mathbf{x} . Conversely, $\mathcal{P}^* = 0$ if and only if $\text{Var}(\mathbb{E}[\mathbf{y} | \mathbf{x}]) = 0$, i.e., the conditional mean $\mathbb{E}[\mathbf{y} | \mathbf{x}]$ is constant and \mathbf{x} conveys no information for predicting the mean of \mathbf{y} .

4 METHOD

4.1 SPECTRAL COHERENCE PREDICTABILITY

Building on the intrinsic predictability in Eq. (4), we seek a computable surrogate from a single realization by leveraging frequency-domain structure. The resulting Spectral Coherence Predictability (SCP) quantifies how much of the future segment \mathbf{y} is linearly explainable by the history segment \mathbf{x} across frequencies, and then aggregates the explained and unexplained power.

We operate in the frequency domain using Welch’s method. Let $\hat{S}_{yy}(f)$ and $\hat{S}_{xx}(f)$ denote the power spectral densities (PSD) of \mathbf{y} and \mathbf{x} , and let $\hat{S}_{xy}(f)$ denote their cross-power spectral density

Algorithm 1 Spectral Coherence Predictability (SCP)

Require: History $\mathbf{x} \in \mathbb{R}^N$, future $\mathbf{y} \in \mathbb{R}^N$; Welch parameters (window, segment length, overlap); stability constant $\varepsilon > 0$; optional frequency band \mathcal{F}_b .

Ensure: MSE linear lower bound MSE_{lb} and predictability \mathcal{P}_{xy} .

- 1: **Mean removal:** $m_x \leftarrow \text{mean}(x)$, $m_y \leftarrow \text{mean}(y)$; $\Delta^2 \leftarrow (m_y - m_x)^2$; $x \leftarrow x - m_x$, $y \leftarrow y - m_y$.
- 2: **Welch spectra:** Compute the PSD $\widehat{S}_{xx}(f)$, $\widehat{S}_{yy}(f)$ and the CPSD $\widehat{S}_{xy}(f)$ on the discrete frequency domain \mathcal{F} .
- 3: **Squared coherence:**

$$\gamma^2(f) \leftarrow \frac{|\widehat{S}_{xy}(f)|^2}{(\widehat{S}_{xx}(f) + \varepsilon)(\widehat{S}_{yy}(f) + \varepsilon)} \in [0, 1], \quad \forall f \in \mathcal{F}.$$

- 4: **Residual spectrum:** $\widehat{S}_e(f) \leftarrow \widehat{S}_{yy}(f)(1 - \gamma^2(f))$, $\forall f \in \mathcal{F}$.
- 5: **Frequency set:** $\mathcal{F}_* \leftarrow \mathcal{F}_b$ if a band \mathcal{F}_b is provided; otherwise $\mathcal{F}_* \leftarrow \mathcal{F}$.
- 6: **Aggregate:**

$$\widehat{\text{Var}}(\mathbf{y}) \leftarrow \sum_{f \in \mathcal{F}_*} \widehat{S}_{yy}(f), \quad \text{MSE}_{\text{lb}} \leftarrow \Delta^2 + \sum_{f \in \mathcal{F}_*} \widehat{S}_e(f).$$

- 7: **Predictability:** $\mathcal{P}_{xy} \leftarrow 1 - \text{MSE}_{\text{lb}}/\widehat{\text{Var}}(\mathbf{y})$.
- 8: **return** MSE_{lb} , \mathcal{P}_{xy} .

(CPSD). All spectra are computed on the same discrete Fourier transform (DFT) grid with identical Welch parameters after mean removal. The squared coherence between \mathbf{y} and \mathbf{x} is

$$\gamma_{xy}^2(f) = \frac{|\widehat{S}_{xy}(f)|^2}{(\widehat{S}_{xx}(f) + \varepsilon)(\widehat{S}_{yy}(f) + \varepsilon)} \in [0, 1], \quad (5)$$

where $\varepsilon > 0$ is a small Tikhonov term for numerical stability. Interpreting $\gamma_{xy}^2(f)$ as a linearly explained–power ratio, the unexplained (residual) spectrum is

$$\widehat{S}_e(f) = \widehat{S}_{yy}(f)(1 - \gamma_{xy}^2(f)). \quad (6)$$

Let \mathcal{F} denote the discrete frequency domain under our normalization, so that the total spectral power equals the sample variance, i.e., $\sum_{f \in \mathcal{F}} \widehat{S}_{yy}(f) = \widehat{\text{Var}}(\mathbf{y})$. To correct a boundary mean mismatch, we optionally add a boundary mean–shift term $\Delta^2 = (\text{mean}(\mathbf{y}) - \text{mean}(\mathbf{x}))^2$. This yields a lower bound on the mean squared error of any linear time–invariant predictor that uses \mathbf{x} :

$$\text{MSE}_{\text{lb}} = \Delta^2 + \sum_{f \in \mathcal{F}} \widehat{S}_e(f), \quad \widehat{\text{Var}}(\mathbf{y}) = \sum_{f \in \mathcal{F}} \widehat{S}_{yy}(f). \quad (7)$$

The SCP estimate of predictability is then

$$\mathcal{P}_{xy} = 1 - \frac{\text{MSE}_{\text{lb}}}{\widehat{\text{Var}}(\mathbf{y})} \in [0, 1]. \quad (8)$$

Algorithm 1 summarizes the steps. Computationally, with fast Fourier transform and Welch estimation, SCP costs $\mathcal{O}(N \log N)$ per sample. This is substantially lower than matching–based Lempel–Ziv–style predictability estimators, which typically entail at least quadratic–to–cubic time in sequence length (e.g., $\mathcal{O}(N^3)$ in naive implementations) and usually target single–step predictability, whereas SCP yields a multi–step estimate aligned with the evaluation horizon.

Theoretical interpretation. If (\mathbf{x}, \mathbf{y}) is jointly Gaussian and wide–sense stationary around the boundary, the Bayes predictor is linear (Ko & Fox, 2009). In this case, Eq. (8) is a consistent estimator of the intrinsic predictability \mathcal{P}_{xy}^* as the effective sample size grows. For general (possibly non-linear) processes, $\widehat{\text{MSE}}_{\text{lb}}$ lower–bounds the error of any linear time–invariant forecaster using \mathbf{x} , hence \mathcal{P}_{xy} is a conservative estimate that isolates the explanatory power of stable linear dynamics across frequencies and sets a meaningful baseline for non-linear forecasters.

Algorithm 2 Linear Utilization Ratio (LUR)

Require: History $\mathbf{x} \in \mathbb{R}^N$, future $\mathbf{y} \in \mathbb{R}^N$, model prediction $\hat{\mathbf{y}} \in \mathbb{R}^N$; Welch parameters (window, segment length, overlap); stability $\varepsilon > 0$; optional frequency band \mathcal{F}_b .

Ensure: Model-explained power P_{model} ; linear-explainable power P_{linear} ; evaluation ratio LUR.

1: **Mean removal:** $\mathbf{x} \leftarrow \mathbf{x} - \text{mean}(\mathbf{x})$; $\mathbf{y} \leftarrow \mathbf{y} - \text{mean}(\mathbf{y})$; $\hat{\mathbf{y}} \leftarrow \hat{\mathbf{y}} - \text{mean}(\hat{\mathbf{y}})$.

2: **Welch spectra (same parameters for all):**

$$\hat{S}_{xx}(f), \hat{S}_{yy}(f), \hat{S}_{\hat{y}\hat{y}}(f), \hat{S}_{xy}(f), \hat{S}_{y\hat{y}}(f), \quad \forall f \in \mathcal{F}.$$

3: **Coherences:**

$$\gamma_{yx}^2(f) \leftarrow \frac{|\hat{S}_{yx}(f)|^2}{(\hat{S}_{yy}(f) + \varepsilon)(\hat{S}_{xx}(f) + \varepsilon)}, \quad \gamma_{y\hat{y}}^2(f) \leftarrow \frac{|\hat{S}_{y\hat{y}}(f)|^2}{(\hat{S}_{yy}(f) + \varepsilon)(\hat{S}_{\hat{y}\hat{y}}(f) + \varepsilon)}.$$

▷ Eq. (5) and Eq. (9).

4: **Frequency set:** $\mathcal{F}_* \leftarrow \mathcal{F}_b$ if a band \mathcal{F}_b is provided; otherwise $\mathcal{F}_* \leftarrow \mathcal{F}$.

5: **Power-weighted aggregation:**

$$P_{\text{model}} \leftarrow \sum_{f \in \mathcal{F}_*} \gamma_{y\hat{y}}^2(f) \hat{S}_{yy}(f), \quad P_{\text{linear}} \leftarrow \sum_{f \in \mathcal{F}_*} \gamma_{yx}^2(f) \hat{S}_{yy}(f).$$

6: **LUR ratio:** $\text{LUR} \leftarrow P_{\text{model}}/P_{\text{linear}}$.

7: **return** P_{model} , P_{linear} , LUR.

4.2 SLINEAR UTILIZATION RATIO

Instead of relying on standard metrics like MSE or MAE, which only tell us if a model is accurate, our approach analyzes why it is accurate by comparing its performance to the data’s theoretical predictability limit in the frequency domain.

Our method, detailed in Algorithm 2, is built on two key quantities: The first key quantity is the linear limit, given by the squared coherence between the future \mathbf{y} and the history \mathbf{x} , $\gamma_{yx}^2(f)$ in Eq. (5), which upper-bounds, at frequency f , the fraction of \mathbf{y} ’s power that any linear predictor can explain using \mathbf{x} . The second quantity is the prediction–target coherence, measuring how much of \mathbf{y} ’s power is actually captured by the model prediction $\hat{\mathbf{y}}$ at frequency f :

$$\gamma_{y\hat{y}}^2(f) = \frac{|\hat{S}_{y\hat{y}}(f)|^2}{(\hat{S}_{yy}(f) + \varepsilon)(\hat{S}_{\hat{y}\hat{y}}(f) + \varepsilon)} \in [0, 1]. \quad (9)$$

Comparing these two coherences yields a per-frequency diagnosis:

- If $\gamma_{y\hat{y}}^2(f) < \gamma_{yx}^2(f)$, the model under-utilizes linearly predictable information in the history \mathbf{x} .
- If $\gamma_{y\hat{y}}^2(f) \approx \gamma_{yx}^2(f)$, the model saturates the linear limit of the history \mathbf{x} .
- If $\gamma_{y\hat{y}}^2(f) > \gamma_{yx}^2(f)$, the model surpasses the linear limit of the history \mathbf{x} , indicating exploitation of nonlinear patterns or additional, correlated data sources.

To summarize over frequency while prioritizing strong signal regions, we weight coherence by the target power spectrum $\hat{S}_{yy}(f)$ on the discrete frequency domain \mathcal{F} . Define the aggregated powers

$$P_{\text{model}} = \sum_{f \in \mathcal{F}} \gamma_{y\hat{y}}^2(f) \hat{S}_{yy}(f), \quad P_{\text{linear}} = \sum_{f \in \mathcal{F}} \gamma_{yx}^2(f) \hat{S}_{yy}(f), \quad (10)$$

The fraction of target energy that is linearly predictable is

$$\eta_{\text{linear}} = \frac{P_{\text{linear}}}{\sum_{f \in \mathcal{F}} \hat{S}_{yy}(f)} = \frac{P_{\text{linear}}}{\widehat{\text{Var}}(\mathbf{y})}. \quad (11)$$

To further assess how much of this predictable energy the model actually captures, we use the Linear Utilization Ratio (LUR)

$$\text{LUR} = \frac{P_{\text{model}}}{P_{\text{linear}}} \geq 0. \quad (12)$$

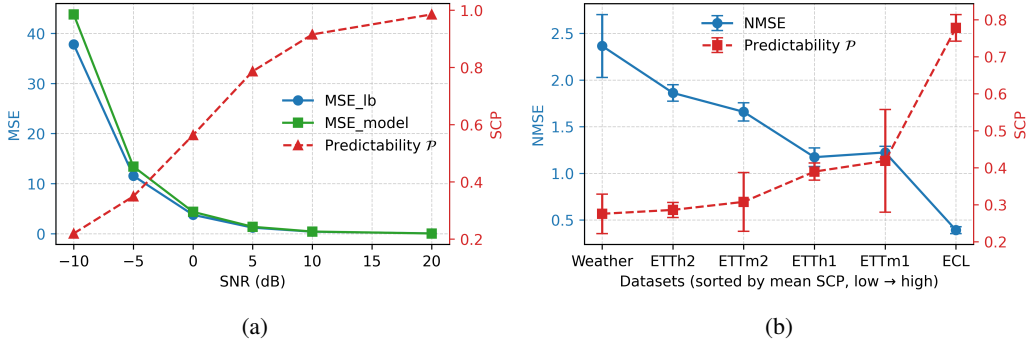


Figure 1: Relationship between model error (MSE) and predictability \mathcal{P} . (a) MSE of the best linear predictor on a synthetic Gaussian process with varying SNR. (b) Average performance of state-of-the-art prediction models on real datasets. We report normalized MSE (NMSE), obtained by dividing MSE by the corresponding variance.

When $LUR < 1$, the model under-exploits linear information available in the history \mathbf{x} ; when $LUR \approx 1$, it saturates the linear limit; when $LUR > 1$, it achieves gains beyond linear structure (e.g., nonlinear dynamics or cross-instance inductive patterns learned from the training set).

To analyze behavior across scales, we additionally partition the discrete frequency domain into disjoint bands $\{\mathcal{F}_b\}_{b=1}^B$ (e.g., low/mid/high), using the band partition as in Algorithms 1 and 2. This yields band-limited counterparts $MSE_{lb,b}$, $\mathcal{P}_{xy,b}$, and LUR_b , which enable localized diagnosis of under-use, saturation, or beyond-linear gains within each frequency band.

5 EXPERIMENTS

This section empirically evaluates our metric and diagnostics across synthetic and real-world settings, guided by three questions: **Q1:** Does our proposed metric accurately reflect the intrinsic predictability of time series data (Secs. 5.1 and 5.2)? **Q2:** What novel insights and observations can be derived from this new metric (Sec. 5.3)? **Q3:** How can our metric be leveraged to enable more comprehensive evaluation methodologies for forecasting models (Secs. 5.4 and 5.5)?

5.1 TOY STUDY

We first validate our proposed predictability score \mathcal{P} and theoretical error lower bound MSE_{lb} in a controlled, synthetic environment. Our setup consists of a Gaussian process with additive noise at varying SNRs, on which we evaluate an optimal linear forecaster (Fig. 1a). For each SNR, we report the model’s test MSE, the estimated linear lower bound MSE_{lb} , and the corresponding predictability \mathcal{P} . As noise decreases (higher SNR), \mathcal{P} increases monotonically toward one, and the model MSE approaches MSE_{lb} . Across all SNRs, MSE_{lb} remains strictly below the realized MSE, confirming it is a valid lower bound; the shrinking gap at high SNR indicates that the linear model saturates the data-implied limit when the process is nearly noise-free. It validates both the calibration (monotonic response to noise) and the tightness (small bound–error gap in the linear regime) of our estimates.

5.2 ALIGNING PREDICTABILITY AND FORECASTING PERFORMANCE

To ensure a fair and rigorous comparison, we evaluate all baselines under a strictly controlled setup: (i) the forecast horizon and the history length are fixed and identical across models; (ii) the common “drop–last” heuristic is disabled. For correlation analyses, we report the Pearson coefficient R between each model’s empirical prediction MSE and the theoretically estimated MSE_{lb} , averaged over all variables and samples in the test set to provide a holistic summary.

As shown in Table 1, MSE_{lb} strongly correlates with the empirical MSE of SOTA models across datasets, with Pearson correlations typically $R \geq 0.8$. This alignment indicates that the bound accurately predicts where forecasting is intrinsically easier or harder, in agreement with realized

Table 1: Long-term multivariate forecasting results. We report MSE, MAE, NMSE for forecasting lengths equal to history length $N \in \{96, 192, 336, 720\}$ under an identical protocol (same preprocessing and no drop-last). **Bold** marks the best (lowest) MSE/MAE per column across models. *Average* rows give the column-wise mean across models. Predictability reports the per-task linear MSE lower bound (MSE_{lb}) and SCP \mathcal{P} (higher is easier).

Models	Metric	ETTh1				ETTh2				ETTm1				ETTm2				ECL				Weather			
		96	192	336	720	96	192	336	720	96	192	336	720	96	192	336	720	96	192	336	720	96	192	336	720
iTransformer (Liu et al., 2024)	MSE	0.387	0.441	0.471	0.700	0.301	0.381	0.426	0.425	0.342	0.345	0.379	0.448	0.186	0.254	0.289	0.382	0.148	0.156	0.170	0.194	0.176	0.214	0.255	0.353
	MAE	0.405	0.440	0.464	0.608	0.350	0.405	0.438	0.455	0.377	0.378	0.403	0.449	0.272	0.319	0.341	0.407	0.239	0.250	0.266	0.287	0.216	0.255	0.290	0.387
	NMSE	1.121	1.095	1.056	1.292	1.598	1.829	1.563	1.432	1.340	1.167	1.140	1.159	1.609	1.696	1.595	1.917	0.288	0.268	0.280	0.319	2.629	2.353	2.032	2.150
	R	0.844	0.876	0.899	0.747	0.907	0.883	0.877	0.842	0.845	0.782	0.803	0.869	0.868	0.834	0.898	0.840	0.723	0.778	0.821	0.826	0.900	0.876	0.801	0.824
TimeMixer (Wang et al., 2024)	MSE	0.381	0.440	0.482	0.631	0.289	0.377	0.390	0.435	0.322	0.337	0.380	0.484	0.176	0.231	0.280	0.376	0.153	0.155	0.172	0.214	0.169	0.198	0.249	0.347
	MAE	0.400	0.434	0.460	0.561	0.340	0.406	0.423	0.458	0.359	0.372	0.396	0.469	0.259	0.296	0.332	0.390	0.245	0.244	0.264	0.310	0.215	0.242	0.291	0.355
	NMSE	1.131	1.069	1.062	1.155	1.540	1.724	1.524	1.446	1.303	1.105	1.125	1.202	1.493	1.485	1.498	1.689	0.282	0.274	0.286	0.334	2.602	2.161	2.107	2.162
	R	0.815	0.889	0.848	0.793	0.916	0.801	0.909	0.906	0.829	0.781	0.752	0.798	0.843	0.867	0.910	0.732	0.706	0.607	0.682	0.887	0.911	0.862	0.885	0.852
DLinear (Zeng et al., 2023)	MSE	0.383	0.422	0.447	0.507	0.329	0.375	0.463	0.740	0.346	0.342	0.372	0.415	0.187	0.242	0.278	0.374	0.195	0.163	0.169	0.197	0.197	0.225	0.263	0.315
	MAE	0.396	0.421	0.448	0.517	0.380	0.410	0.472	0.609	0.374	0.369	0.389	0.415	0.281	0.315	0.338	0.406	0.277	0.259	0.268	0.295	0.255	0.282	0.314	0.354
	NMSE	1.214	1.143	1.310	1.782	2.927	2.067	2.728	3.896	1.327	1.205	1.208	1.121	1.676	1.722	1.620	1.793	0.868	0.678	0.574	0.684	3.507	2.899	2.474	2.069
	R	0.869	0.878	0.872	0.804	0.845	0.880	0.798	0.439	0.868	0.887	0.819	0.884	0.833	0.813	0.910	0.902	0.880	0.867	0.909	0.864	0.924	0.931	0.911	0.922
PatchTST (Nie et al., 2023)	MSE	0.391	0.429	0.436	0.465	0.293	0.357	0.363	0.406	0.322	0.328	0.365	0.417	0.177	0.230	0.276	0.356	0.167	0.151	0.167	0.212	0.176	0.202	0.247	0.309
	MAE	0.403	0.426	0.440	0.482	0.342	0.387	0.402	0.442	0.358	0.364	0.390	0.419	0.258	0.294	0.329	0.385	0.252	0.242	0.258	0.304	0.217	0.243	0.281	0.331
	NMSE	1.205	1.227	1.113	1.341	1.952	2.115	1.556	1.527	1.391	1.424	1.352	1.361	1.714	1.621	1.933	2.012	0.316	0.345	0.350	0.482	2.555	2.531	2.294	2.055
	R	0.869	0.881	0.915	0.876	0.886	0.920	0.911	0.864	0.813	0.652	0.741	0.835	0.904	0.908	0.863	0.909	0.735	0.809	0.737	0.969	0.912	0.903	0.868	0.865
TimesNet (Wu et al., 2023)	MSE	0.389	0.460	0.487	0.641	0.337	0.405	0.399	0.447	0.334	0.414	0.429	0.482	0.189	0.239	0.320	0.383	0.168	0.189	0.209	0.305	0.169	0.220	0.272	0.334
	MAE	0.412	0.456	0.477	0.582	0.371	0.424	0.433	0.463	0.375	0.414	0.434	0.477	0.266	0.306	0.357	0.408	0.272	0.291	0.308	0.382	0.219	0.265	0.301	0.350
	NMSE	1.205	1.227	1.113	1.341	1.952	2.115	1.556	1.527	1.391	1.424	1.352	1.361	1.714	1.621	1.933	2.012	0.316	0.345	0.350	0.482	2.555	2.531	2.294	2.055
	R	0.869	0.881	0.915	0.876	0.886	0.920	0.911	0.864	0.813	0.652	0.741	0.835	0.904	0.908	0.863	0.909	0.735	0.809	0.737	0.969	0.912	0.903	0.868	0.865
Average	MSE	0.386	0.438	0.465	0.589	0.310	0.379	0.408	0.491	0.333	0.353	0.385	0.449	0.183	0.239	0.289	0.374	0.166	0.163	0.177	0.224	0.177	0.212	0.257	0.332
	MAE	0.403	0.435	0.458	0.550	0.357	0.406	0.434	0.485	0.369	0.379	0.402	0.446	0.267	0.306	0.339	0.399	0.257	0.257	0.273	0.316	0.224	0.257	0.295	0.349
	NMSE	1.149	1.120	1.105	1.321	1.912	1.863	1.738	1.936	1.321	1.199	1.193	1.184	1.608	1.599	1.626	1.805	0.415	0.366	0.356	0.432	2.814	2.421	2.179	2.047
Predictability	MSE_{lb}	0.354	0.417	0.404	0.412	0.298	0.360	0.309	0.356	0.228	0.307	0.513	0.436	0.175	0.248	0.295	0.361	0.239	0.219	0.167	0.241	0.185	0.244	0.278	0.317
	\mathcal{P}	0.422	0.379	0.368	0.389	0.305	0.270	0.302	0.267	0.590	0.460	0.268	0.356	0.415	0.315	0.230	0.271	0.751	0.755	0.829	0.777	0.345	0.240	0.228	0.289

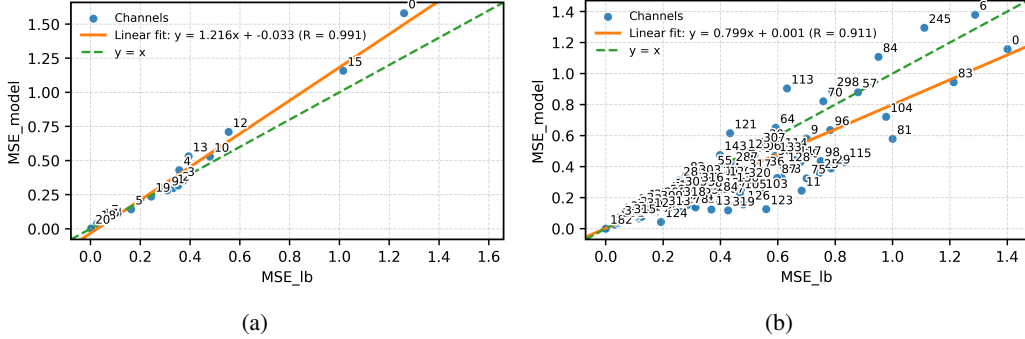


Figure 2: Per-variable scatter plots on Weather (a) and ECL (b) comparing the estimated MSE lower bound (MSE_{lb}) with iTransformer’s prediction error ($\text{MSE}_{\text{model}}$).

model accuracy. To visualize this relationship, Fig. 2 plots iTransformer’s MSE against MSE_{lb} for each channel in ECL and Weather datasets, revealing a near-linear trend. Collectively, these dataset- and channel-level results validate the effectiveness of our MSE_{lb} estimator. They also highlight substantial within-dataset heterogeneity: predictability and MSE can vary markedly across channels.

To compare predictability across datasets, we aggregate over horizons and report, for each dataset, the mean \pm std of SCP \mathcal{P} and realized NMSE (Fig. 1b). The relationship is strongly inverse: datasets with higher \mathcal{P} tend to exhibit lower NMSE on average. In particular, ECL shows the highest \mathcal{P} and the lowest NMSE (easiest to forecast), whereas Weather exhibits the lowest \mathcal{P} and the highest NMSE (hardest). This ordering indicates that \mathcal{P} ranks dataset difficulty in a manner that aligns with realized errors.

Overall, no single architecture dominates across all datasets and horizons—an expected outcome in predictability-limited settings that, as shown later, arises from time- and band-dependent variability in the exploitable history x that challenges both linear and nonlinear representations.

5.3 TIME-VARYING PREDICTABILITY

Standard evaluation metrics, which average performance over an entire test set, implicitly assume that the forecasting task is statistically stationary. However, this assumption often fails for time series tasks. Focusing on a single channel, we move sample by sample, plotting two key metrics in parallel: the model’s instantaneous error (MSE) and our measure of the data’s predictable energy, decomposed by frequency.

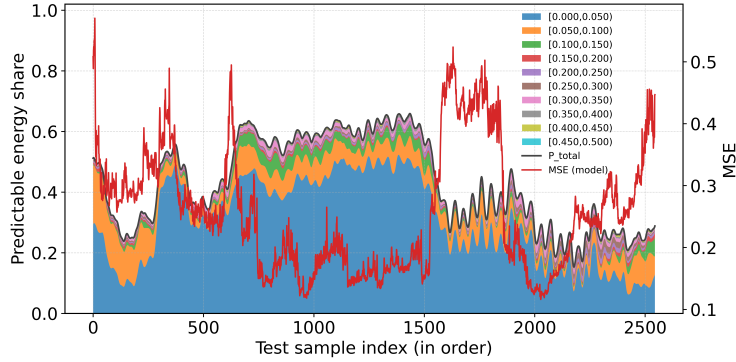


Figure 3: ETTh1 test set, channel 1, horizon $N = 96$. Relationship between per-sample linearly predictable energy (decomposed by frequency band as a share of total) and DLinear’s MSE.

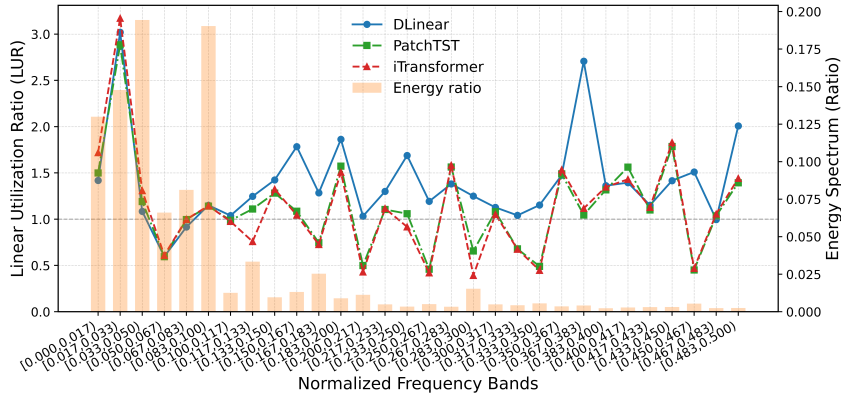


Figure 4: Band-wise analysis on ETTh1, representative channel. Normalized energy shares and LUR across frequency bands for three models.

The results, shown in Fig. 3, are striking. We find that a model’s performance is not random but is tightly coupled to the instantaneous predictable energy in the data. This reveals that predictability is not a fixed property of a dataset; it varies sharply from one moment to the next. This phenomenon, which we term predictability drift, means the forecasting task should be viewed not as a single problem, but as a time-varying mixture of easy and hard regimes.

When the total predictable share is low, or when the dominant predictable bands shift rapidly, MSE spikes. These observations explain why aggregate test-set statistics often fail to discriminate models. Fluctuations in sample-level predictability always dominate realized error. They also motivate finer-grained evaluation protocols, such as band-wise diagnostics and predictability-aware reporting, which enable grouping evaluations conditioned on data characteristics and provide actionable guidance for model development.

5.4 BAND-WISE EVALUATION

To gain a more granular understanding, we use the Linear Utilization Ratio (LUR) to analyze model behavior in the frequency domain. We decompose the test signal into distinct frequency bands and, for each band, measure both the proportion of the signal’s total energy and the LUR for several representative models.

Figure 4 reveals the distinct strategies employed by different model architectures. In the five low-frequency bands, which contain the majority of the signal’s energy, all three models exhibit a similar pattern: their LURs closely track the energy distribution. This indicates that all models correctly identify and attempt to capture these dominant, high-energy components of the signal. Within these

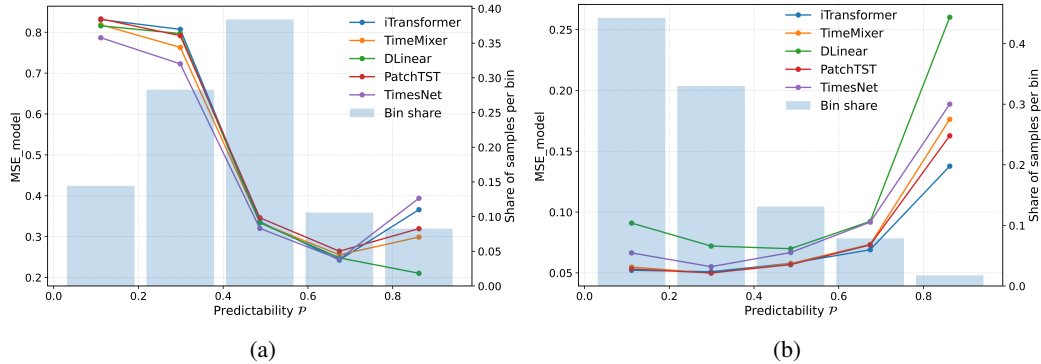


Figure 5: ETTh1 dataset with forecasting length $N = 96$: per-channel evaluation stratified by predictability \mathcal{P} . Samples are grouped into equal-width \mathcal{P} bins; each point reports the mean MSE within the bin.

critical bands, however, the PatchTST and iTransformer achieve a slightly higher LUR than DLinear, suggesting they are more efficient at extracting information from these primary signal components.

A more significant divergence appears in the higher-frequency bands. Here, DLinear maintains a significantly higher LUR than both PatchTST and iTransformer. This finding exposes the fundamental difference in their underlying mechanisms. DLinear, being a simple linear model, acts like a broadband filter, attempting to capture information indiscriminately across the entire spectrum. In contrast, Transformer-based models like PatchTST and iTransformer function as frequency-selective filters. They intelligently focus their capacity on the high-energy, low-frequency bands where the most predictable signal resides, while largely ignoring the less informative, high-frequency noise. This demonstrates their more sophisticated inductive bias for typical time-series data.

5.5 PREDICTABILITY-AWARE EVALUATION

Although most models achieve a similar MSE of ≈ 0.38 on the ETTh1 dataset (horizon $N = 96$), this average score obscures critical performance differences. By stratifying the test set by our predictability score \mathcal{P} , we uncover these hidden behaviors (Fig. 5). In Fig. 5a, complex nonlinear forecasters (e.g., TimesNet, TimeMixer) perform better in the low- \mathcal{P} bin (hard samples), whereas DLinear outperforms in the high- \mathcal{P} (easy samples) bin. In Fig. 5b, where samples concentrate in the low- \mathcal{P} region, iTransformer, TimeMixer, and PatchTST exhibit convergent performance, while DLinear is capacity-limited on hard cases and tends to underfit easy cases due to their low ratio. These contrasts highlight complementary strengths across architectures: nonlinear models excel when the linear predictable signal is scarce, whereas simple linear models are highly competitive when predictability is high.

6 CONCLUSION AND FUTURE WORK

This work confronts a fundamental flaw in time series forecasting evaluation: the conflation of model error with intrinsic data difficulty. We introduced a predictability-aligned diagnostic framework, centered on the Spectral Coherence Predictability (SCP) score and the Linear Utilization Ratio (LUR), to disentangle these factors. Our analysis not only provided the first systematic evidence of “predictability drift” but also revealed that different architectures possess complementary strengths, a nuance lost in aggregate metrics. Ultimately, our contribution is a call to shift the community’s focus from simplistic model rankings to a more insightful, diagnostic approach. This paradigm change fosters a deeper understanding of model behavior, enables fairer comparisons, and paves the way for the development of more robust and targeted forecasting solutions. Looking ahead, our framework opens the door to new data-aware learning paradigms. For instance, the SCP score can guide curriculum learning strategies by ordering data by difficulty, while the LUR could serve as a novel regularizer, paving the way for more adaptive and robust forecasting systems.

ETHICS STATEMENT

This work does not introduce new data collection involving human subjects. All experiments use publicly available datasets (ETT, Weather, ECL) under their original licenses and terms of use; no sensitive attributes (e.g., protected classes or personally identifiable information) are inferred or used. Our analyses operate on aggregated forecasting errors and frequency-domain summaries, not on individual-level predictions tied to identity or behavior.

REPRODUCIBILITY STATEMENT

We aim for full reproducibility and have released all code, configurations, and scripts to reproduce our results, including data preparation, backbone training/evaluation, and the SCP/LUR diagnostics.

REFERENCES

- Mateo Aboy, Roberto Hornero, Daniel Abásolo, and Daniel Álvarez. Interpretation of the Lempel-Ziv complexity measure in the context of biomedical signal analysis. *IEEE transactions on biomedical engineering*, 53(11):2282–2288, 2006.
- Christoph Bandt and Bernd Pompe. Permutation Entropy: A Natural Complexity Measure for Time Series. *Physical Review Letters*, 88(17):174102, April 2002. ISSN 0031-9007, 1079-7114. doi: 10.1103/PhysRevLett.88.174102.
- Christoph Bergmeir. Fundamental limitations of foundational forecasting models: The need for multimodality and rigorous evaluation. In *Proc. NeurIPS Workshop*, 2024.
- Xi Chen, Adityanand Guntuboyina, and Yuchen Zhang. On Bayes risk lower bounds. *Journal of Machine Learning Research*, 17(218):1–58, 2016.
- Andrew SC Ehrenberg and John A. Bound. Predictability and prediction. *Journal of the Royal Statistical Society Series A: Statistics in Society*, 156(2):167–194, 1993.
- Miro Erkintalo. Predicting the unpredictable? *Nature Photonics*, 9(9):560–562, 2015.
- Mark Fiecas, Chenlei Leng, Weidong Liu, and Yi Yu. Spectral analysis of high-dimensional time series. 2019.
- Joshua Garland, Ryan James, and Elizabeth Bradley. Model-free quantification of time-series predictability. *Physical Review E*, 90(5):052910, November 2014. ISSN 1539-3755, 1550-2376. doi: 10.1103/PhysRevE.90.052910.
- Marta C. González, César A. Hidalgo, and Albert-László Barabási. Understanding individual human mobility patterns. *Nature*, 453(7196):779–782, June 2008. ISSN 1476-4687. doi: 10.1038/nature06958.
- Jonathan Ko and Dieter Fox. GP-BayesFilters: Bayesian filtering using Gaussian process prediction and observation models. *Autonomous Robots*, 27(1):75–90, July 2009. ISSN 0929-5593, 1573-7527. doi: 10.1007/s10514-009-9119-x.
- Ioannis Kontoyiannis, Paul H. Algoet, Yu M. Suhov, and Abraham J. Wyner. Nonparametric entropy estimation for stationary processes and random fields, with applications to English text. *IEEE transactions on information theory*, 44(3):1319–1327, 2002.
- Shiyang Li, Xiaoyong Jin, Yao Xuan, Xiyu Zhou, Wenhui Chen, Yu-Xiang Wang, and Xifeng Yan. Enhancing the Locality and Breaking the Memory Bottleneck of Transformer on Time Series Forecasting. In *Advances in Neural Information Processing Systems*, volume 32. Curran Associates, Inc., 2019.
- Yong Liu, Tengge Hu, Haoran Zhang, Haixu Wu, Shiyu Wang, Lintao Ma, and Mingsheng Long. iTransformer: Inverted Transformers Are Effective for Time Series Forecasting. In *The Thirteenth International Conference on Learning Representations*. The Thirteenth International Conference on Learning Representations, March 2024.

- Sakshi Mishra and Praveen Palanisamy. Multi-time-horizon solar forecasting using recurrent neural network. In *2018 IEEE Energy Conversion Congress and Exposition (ECCE)*, pp. 18–24. IEEE, 2018.
- Jamal Mohammed, Michael H. Böhlen, and Sven Helmer. Quantifying and Estimating the Predictability Upper Bound of Univariate Numeric Time Series. In *Proceedings of the 30th ACM SIGKDD Conference on Knowledge Discovery and Data Mining, KDD '24*, pp. 2236–2247, New York, NY, USA, August 2024. Association for Computing Machinery. ISBN 979-8-4007-0490-1. doi: 10.1145/3637528.3671995.
- Yuqi Nie, Nam H. Nguyen, Phanwadee Sinthong, and Jayant Kalagnanam. A Time Series is Worth 64 Words: Long-term Forecasting with Transformers. arXiv, March 2023. doi: 10.48550/arXiv.2211.14730.
- Frank Pennekamp, Alison C. Iles, Joshua Garland, Georgina Brennan, Ulrich Brose, Ursula Gaedke, Ute Jacob, Pavel Kratina, Blake Matthews, Stephan Munch, Mark Novak, Gian Marco Palamara, Björn C. Rall, Benjamin Rosenbaum, Andrea Tabi, Colette Ward, Richard Williams, Hao Ye, and Owen L. Petchey. The intrinsic predictability of ecological time series and its potential to guide forecasting. *Ecological Monographs*, 89(2):e01359, May 2019. ISSN 0012-9615, 1557-7015. doi: 10.1002/ecm.1359.
- S M Pincus. Approximate entropy as a measure of system complexity. *Proceedings of the National Academy of Sciences*, 88(6):2297–2301, March 1991. ISSN 0027-8424, 1091-6490. doi: 10.1073/pnas.88.6.2297.
- Joshua S. Richman and J. Randall Moorman. Physiological time-series analysis using approximate entropy and sample entropy. *American Journal of Physiology-Heart and Circulatory Physiology*, 278(6):H2039–H2049, June 2000. ISSN 0363-6135, 1522-1539. doi: 10.1152/ajpheart.2000.278.6.H2039.
- C. E. Shannon. A mathematical theory of communication. *The Bell System Technical Journal*, 27(3):379–423, July 1948. ISSN 0005-8580. doi: 10.1002/j.1538-7305.1948.tb01338.x.
- Chaoming Song, Zehui Qu, Nicholas Blumm, and Albert-László Barabási. Limits of predictability in human mobility. *Science*, 327(5968):1018–1021, February 2010. doi: 10.1126/science.1177170.
- Huandong Wang, Sihan Zeng, Yong Li, and Depeng Jin. Predictability and Prediction of Human Mobility Based on Application-Collected Location Data. *IEEE Transactions on Mobile Computing*, 20(7):2457–2472, July 2021. ISSN 1558-0660. doi: 10.1109/TMC.2020.2981441.
- Yuxuan Wang, Haixu Wu, Jiayang Dong, Guo Qin, Haoran Zhang, Yong Liu, Yunzhong Qiu, Jianmin Wang, and Mingsheng Long. TimeXer: Empowering Transformers for Time Series Forecasting with Exogenous Variables. In *The Thirty-eighth Annual Conference on Neural Information Processing Systems*, November 2024.
- Haixu Wu, Jiehui Xu, Jianmin Wang, and Mingsheng Long. Autoformer: Decomposition transformers with auto-correlation for long-term series forecasting. *Advances in neural information processing systems*, 34:22419–22430, 2021.
- Haixu Wu, Tengge Hu, Yong Liu, Hang Zhou, Jianmin Wang, and Mingsheng Long. TimesNet: Temporal 2D-Variation Modeling for General Time Series Analysis, April 2023.
- Aaron D. Wyner and Jacob Ziv. Some asymptotic properties of the entropy of a stationary ergodic data source with applications to data compression. *IEEE Transactions on Information Theory*, 35(6):1250–1258, 2002.
- Ailing Zeng, Muxi Chen, Lei Zhang, and Qiang Xu. Are Transformers Effective for Time Series Forecasting? *Proceedings of the AAAI Conference on Artificial Intelligence*, 37(9):11121–11128, June 2023. ISSN 2374-3468. doi: 10.1609/aaai.v37i9.26317.
- Kai Zhao, Denis Khryashchev, and Huy Vo. Predicting Taxi and Uber Demand in Cities: Approaching the Limit of Predictability. *IEEE Transactions on Knowledge and Data Engineering*, 33(6):2723–2736, June 2021. ISSN 1558-2191. doi: 10.1109/TKDE.2019.2955686.

Haoyi Zhou, Shanghang Zhang, Jieqi Peng, Shuai Zhang, Jianxin Li, Hui Xiong, and Wancai Zhang. Informer: Beyond efficient transformer for long sequence time-series forecasting. In *Proceedings of the AAAI Conference on Artificial Intelligence*, volume 35, pp. 11106–11115, 2021.

Tian Zhou, Ziqing Ma, Qingsong Wen, Xue Wang, Liang Sun, and Rong Jin. Fedformer: Frequency enhanced decomposed transformer for long-term series forecasting. In *International Conference on Machine Learning*, pp. 27268–27286. PMLR, 2022.

J. Ziv and A. Lempel. A universal algorithm for sequential data compression. *IEEE Transactions on Information Theory*, 23(3):337–343, May 1977. ISSN 1557-9654. doi: 10.1109/TIT.1977.1055714.

A USAGE OF LLMs

We utilized a large language model (LLM) to proofread and improve the grammatical clarity of this manuscript. All scientific ideas, methodologies, and conclusions presented are the original work of the authors.

B LIMITATIONS AND OPPORTUNITIES

Our estimates rely on windowed Welch spectra and second-order stationarity within windows; the linear limit is conservative for nonlinear/exogenous dynamics. Extending SCP/LUR to multivariate forecasting, multi-step decision feedback, active learning, and hard-sample mining are promising directions.

C EXPERIMENTAL SETUP

C.1 TOY STUDY

We synthesize a multiband Gaussian process and evaluate linear forecasting under controlled band-limited noise. Signals are split into history/future with boundary-paired segments of length $N_p = 512$ from a total length $2N$ with $N = 1024$. Power spectra and coherences are estimated via Welch’s method (Hann window) with $n_{\text{perseg}} = 256$ and $n_{\text{overlap}} = 128$. The forecaster is a causal FIR least-squares filter (Wiener approximation) of length $L_{\text{FIR}} = 64$ with ridge 10^{-6} . The base process has four spectral peaks at rFFT bins $\{32, 96, 192, 384\}$ with widths $\{6, 10, 14, 18\}$ and amplitudes $\{3.0, 2.0, 1.5, 1.0\}$. We sweep noise levels $\{0, 0.25, 0.5, 1.0, 2.0, 4.0\}$ on a single band (index 1 in the plot) and average over 3 trials, reporting model MSE, MSE_{lb} , and SCP.

C.2 BACKBONE

We evaluate seven state-of-the-art backbones spanning diverse architectures: Transformer-based (iTransformer (Liu et al., 2024), PatchTST (Nie et al., 2023)), MLP-based (DLinear (Zeng et al., 2023), TimeMixer (Wang et al., 2024)), and CNN-based (TimesNet (Wu et al., 2023)). We adopt the official implementations and recommended hyperparameters from their repositories. To ensure strict comparability, we fix the forecasting horizon and enforce equal input and output lengths for all backbones (no “drop-last”), using identical preprocessing and dataset splits across models.

C.3 DATASETS

- **ETT (Electricity Transformer Temperature).** ETT records seven variables from electricity transformers collected in two regions between July 2016 and July 2018. Variants differ in sampling granularity: “h” denotes hourly data and “m” denotes 15-minute data; suffixes “1/2” indicate the two regions (ETT_{h1}/ETT_{h2}, ETT_{m1}/ETT_{m2}) (Zhou et al., 2021).
- **Weather.** Weather contains 21 meteorological variables measured every 10 minutes during 2020 at the Max Planck Biogeochemistry Institute’s weather station (Zhou et al., 2021).
- **ECL (Electricity Consuming Load).** ECL provides hourly electricity consumption for 321 clients from 2012 to 2014 (Li et al., 2019).

C.4 TIME-TO-FREQUENCY

For each test instance we split the sequence into history \mathbf{x} and future \mathbf{y} (equal lengths by default), remove sample means, and estimate power and cross-spectra with Welch’s method using identical settings for \mathbf{x} , \mathbf{y} , and (when available) $\hat{\mathbf{y}}$: Hann window with length $n_{\text{win}} = \lfloor 0.25N \rfloor$, 50% overlap, and real FFT on the one-sided grid \mathcal{F} with variance-preserving normalization. We form squared coherences with a small ridge ε for stability, compute the residual spectrum to obtain the linear lower bound MSE_{lb} and predictability $\mathcal{P} = 1 - \text{MSE}_{\text{lb}}/\text{Var}(\mathbf{y})$, and derive utilization metrics (global or band-wise) via target-power-weighted aggregation of $\gamma_{\hat{\mathbf{y}}\hat{\mathbf{y}}}^2$ and $\gamma_{\hat{\mathbf{y}}\mathbf{x}}^2$.